

An Adaptive Registration Algorithm for Zebrafish Larval Brain Images

Shoureen Deb^a, Natascia Tiso^b, Enrico Grisan^{c,d}, Ananda S. Chowdhury^a

^a*Dept. of Electronics and Telecommunication Engineering, Jadavpur University, Kolkata, India*

^b*Department of Biology, University of Padova, Italy*

^c*Department of Information Engineering, University of Padova, Italy*

^d*School of Engineering, London South Bank University, UK*

Abstract

Background and Objective

Zebrafish (*Danio rerio*) in their larval stages have grown increasingly popular as excellent vertebrate models for neurobiological research. Researchers can apply various tools in order to decode the neural structure patterns which can aid the understanding of vertebrate brain development. In order to do so, it is essential to map the gene expression patterns to an anatomical reference precisely. However, high accuracy in sample registration is sometimes difficult to achieve due to laboratory- or protocol-dependent variabilities.

Methods

In this paper, we propose an accurate adaptive registration algorithm for volumetric zebrafish larval image datasets using a synergistic combination of attractive Free-Form-Deformation (FFD) and diffusive Demons algorithms. A coarse registration is achieved first for 3D volumetric data using a 3D

affine transformation. A localized registration algorithm in form of a B-splines based FFD is applied next on the coarsely registered volume. Finally, the Demons algorithm is applied on this FFD registered volume for achieving fine registration by making the solution noise resilient.

Results

Experimental procedures are carried out on a number of 72 hpf (hours post fertilization) 3D confocal zebrafish larval datasets. Comparisons with state-of-the-art methods including some ablation studies clearly demonstrate the effectiveness of the proposed method.

Conclusion

Our adaptive registration algorithm significantly aids Zebrafish imaging analysis over current methods for gene expression anatomical mapping, such as Vibe-Z. We believe the proposed solution would be able to overcome the requirement of high quality images which currently limits the applicability of Zebrafish in neuroimaging research.

Keywords: Zebrafish Imaging, Adaptive Registration, FFD-Demons

Synergism

1. Introduction

A rapid proliferation in terms of behavioral research with the teleost zebrafish (*Danio rerio*) has evolved significantly over the past decade, which has led to zebrafish emerging as a potential vertebrate model for neurocognitive function. Zebrafish have indeed successfully modelled many diseases like Autism, Alzheimer’s, Schizophrenia, drug abuse and other neurological diseases related to cognitive dysfunction, as discussed in [10] and the references within. The reason for this growing popularity in zebrafish models lies in their complex sensory and motor systems which are quintessential for sophisticated learning experiments. Zebrafish larvae have developed into an ideal research model for bio-imaging in vertebrates due to their relative transparency. The zebrafish larval brain contains roughly 10^5 neurons. Thus, a wide range of genetic tools as stated in [35] can be applied by researchers in order to decode the patterns of neural connectivity and structure.

In the present work, we aim at making the registration pipeline adaptive by using a synergistic combination of B-splines based Free Form Deformation (FFD), an attractive model and Demons, a diffusive model. The task at our hand is to register multi-view confocal 3D images of 72 hpf (hours post fertilization) zebrafish larvae on an anatomical reference dataset. Photoacoustic imaging is an extremely powerful strategy when applied to the zebrafish larva, as the transparency of the organism can be fully exploited for a non-invasive imaging of morphological and hemodynamic features *in vivo*. However, this technique and its improvements are a bit out of the scope for this manuscript.

Indeed, our objective is the digital improvement of confocal microscopy images obtained from fixed embryos/larvae, where specific gene expression is stained with post-mortem techniques. The final goal is the correction of possible deformations that prevent the processing of the images by the Vibe-Z software. The Vibe-Z system expects standard sizes for embryos/larvae imaged at specific developmental stages, in order to easily compare them with an internal reference database of gene expression markers previously mapped in age-matched samples. We first capture the global motion of the volume to be registered using a 3D affine registration strategy optimized using the OnePlusOne Evolutionary optimizer [5]. Following the global alignment, the localized registration is performed in which a mesh of control points is used to model the underlying deformations which act as parameters to the B-spline Free Form Deformation (FFD) function [6]. The density of the control mesh is increased in a coarse-to-fine fashion. Note that as the control points model the deformations in the different regions of the zebrafish, they become inherently adaptive. In contrast to Thin Plate Splines (TPS) [8], B-splines are deformed locally resulting in high computational efficiency for a large number of control points. Moreover, the basis functions of cubic B-splines possess limited support which can influence only the local neighbourhood of the control points. The cost function is iteratively minimised using the L-BFGS (Limited Memory Broyden–Fletcher–Goldfarb–Shanno) algorithm. Finally, the demons algorithm [7] is applied to fine tune any of the anomalies which might have existed in the structuring of the control points. The

greatest advantage of our pipeline is that the varying degrees of freedom of the various regions of a zebrafish larva are adaptively captured by varying densities of the control points in the FFD algorithm. Moreover, the final output of the demons algorithm, which also models displacement fields which will vary in accordance with the regions having higher deformity and would automatically fine-tune the output obtained from the FFD algorithm.

We have not considered the intensity of the signal, by the way easily adjustable during or after the imaging of the sample, as this aspect is usually not a critical issue. As long as the marker under consideration is displaying its expected pattern - based on literature information - this is correctly processed by the program. The main issue is the shape and the orientation of the imaged sample, which can indeed depend on laboratory variabilities (especially on the ability of the user to correctly mount the specimen) and protocol variabilities (for instance the softness of the larva after the staining procedure, or the density of the mounting medium, that can affect larval shape and maintenance of the correct position). We now summarize our contributions below:

1. We solve an important biological problem of accurately registering zebrafish larval images to an anatomical reference dataset. The problem has several widespread applications in developmental neurology. To the best of our knowledge, this is the first detailed work of non-rigid registration of zebrafish larval images. The final goal is the standardization of zebrafish images in terms of position and orientation, so that they

can be an adequate input for freeware applications like Vibe-Z, which, by managing anatomical databases, and comparing different reference markers among each other, expect highly standardized body dimensions and shapes.

2. Methodologically speaking, we develop an adaptive strategy for a complex non-rigid registration problem by proposing a synergism between attractive B-Spline based FFD and diffusive Demons algorithms following an affine registration procedure. In our solution, we have changed the similarity measure of the B-Spline based FFD.

The rest of the paper is organized as follows: in Section 2, we discuss the related works. In Section 3, we describe our proposed model in details. In Section 4, we present the experimental results with detailed analysis. Finally, the paper is concluded in section 5 with an outline of directions for future research.

2. Related Work

In this section, we discuss prominent registration algorithms without and with learning having a focus on biomedical applications. This is followed by analysis of some works explicitly dealing with zebrafish registration.

2.1. Registration without Learning

Extensive work has been carried out over the years in 3D medical image registration [11], [12]-[15], [31]. These methods in principle perform an

optimization within the space of displacement vector fields. Examples are spline based FFD [6], statistical parametric mapping [12], Demons [7] and discrete methods [13]. Among these algorithms, the methods conforming to diffeomorphic transforms have shown remarkable success in studies pertaining to computational anatomy as they preserve topology. While optimizing an energy function for a given pair of images these methods require computational time, especially if a large dataset, like ours, is to be registered. In [39], geometric alignment of two roughly preregistered, partially overlapping, rigid, noisy 3D point sets is dealt with by adopting least trimmed squares (LTS) approach in all phases of the operation of the Iterative Closest Point algorithm. In [40], an algorithm for registering RGB point cloud data. It is an enhancement of the iterative close point algorithm with features of salient object detection and maximum correntropy criterion in order to handle with noise and outliers. In [41] correntropy is introduced into the rigid registration problem similar to [40] following which and then a new energy function based on maximum correntropy criterion is proposed. These algorithm, however, would not be robust enough to handle Zebrafish larval image registration simply because of the varying degrees of freedom in the zebrafish larva unlike simple RGB point cloud data.

2.2. Learning Based Registration

There have been several recent studies on Image registration which have proposed neural networks to learn a function for achieving the registration.

A common feature of most of these networks lies in the fact that they use ground truth warp fields ([16] - [20]). Thus, even though these methods appear to be an attractive solution to the image registration problem, ground truth warp fields are difficult to acquire. In [16], Cao *et al.* have implemented a regression model based on convolutional neural networks (CNN) in order to learn the complex mapping from between the input image pair and the deformation fields corresponding to them. The design of the CNN architecture is patch-based to allow the network to learn from the input patch pairs to their corresponding displacement fields. In [37], a multi-objective optimization algorithm based on clustering calculation has been used to perform medial image registration tests. In [42], the technique performs end-to-end training from image pairs to learn priors over geometric transformations and regularities of the 3D world. It uses an attention based context aggregation mechanism, enabling the algorithm to reason about the underlying 3D scene and feature assignments jointly. In order to facilitate accurate CNN model learning, the authors have implemented an equalized active-points guided sampling strategy. An auxiliary contextual cue is added as the similarity metric between the input patches. However, in all cases in which the ground truth warp field is not available (as in our case), any supervised learning based approach cannot be adopted. In [21],[37], an unsupervised learning based registration approach named Voxelmorph determines a registration field based on the moving volumes of the brain CT scans and the weights are learned accordingly. Voxelmorph being an unsupervised learning algorithm

does not need the ground truth labels but it formulates registration as a function that maps an input image pair to a deformation field that aligns these images. Voxelmorph parameterizes the function via a convolutional neural network (CNN), and optimizes the parameters of the neural network on a set of images. Given a new pair of scans, VoxelMorph rapidly computes a deformation field by directly evaluating the function. Thus, Voxelmorph needs a significant amount of computational data in order to parameterize the deformation field. The experiments using Voxelmorph which demonstrate its inadequacy in handling Zebrafish Larval Image registration with limited data has been illustrated in figure 7.

In [1], the registration strategy applied is that of a landmark-based approach which is heavily dependent on the resolution of the underlying image to be registered, owing to which a low image resolution can heavily degrade the quality of registration. Moreover, ViBE-Z also possesses limitations on applications in a large scale as it requires a high level of accuracy and standardization for any new image data produced by numerous laboratories globally. In order to overcome the limitations of [1], Ghosal *et al.* in [2] have adopted a four-step intensity based non-rigid registration algorithm in which the given volume is coarsely registered by means of the L-BFGS optimization method followed by a patch-based fine registration using the Diffeomorphic Demons algorithm and inter-patch regularization. However, the nature of their pipeline comprising the patch-based registration does not take into account the underlying geometry as different regions of the zebrafish larva will

typically have different degrees of freedom and hence would ideally require an adaptive registration strategy.

3. Proposed Method

Image Registration aims at finding an optimal transformation $\mathbb{T} : (x, y, z) \mapsto (x', y', z')$ which establishes a mapping of any given point in the moving image $I'(x', y', z')$ to the corresponding point in the reference image $I(x, y, z)$. The structure of the zebrafish larva, in general is non-rigid with varying degrees of freedom. So, a single affine transformation alone is not at all sufficient in correcting the motion. The head of a larval zebrafish is mostly rigid while the tail can bend and deform heavily thereby exhibiting high non-rigidity. Hence, we propose in this paper an adaptive approach that can cater to the global as well as local transformations. The proposed method consists of three major steps, namely, i) a coarse affine registration, ii) FFD based adaptive local alignment, and iii) Demons based fine registration. The above three steps are first discussed in details. We then explicitly discuss the rationale behind the FFD-Demons synergism. We end this section with an algorithm (Algorithm 1) showing the different steps.

3.1. Global Alignment

In order to capture the overall motion of the moving volume, an affine transformation is applied which parameterizes a rigid transformation comprising 6 degrees of freedom and an additional 6 degrees of freedom modelling

shearing and scaling. The one-plus-one evolutionary optimizer by Styner et al [5] has been used to parameterize the transformation.

3.2. Adaptive Local Alignment

The affine transformation performed in the previous step fails to capture the underlying geometry and the varying degrees of freedom in the underlying moving volume. As the nature of local deformations may vary from one sample to another, applying parameterized transformations for characterizing the local deformations would not suffice. Thus, we use a B-splines [9] based FFD function developed by Rueckert *et al.* [6]. The basic principle of the B-spline based FFD algorithm is that the moving volume is aligned to the reference volume (atlas) by manipulating an underlying mesh of control points. The deformations of the control points take place on the basis of varying degrees of freedom as the regions having higher degrees of freedom would have a higher density of control points leading to smooth and continuous C^2 transformation. We specify the domain of the volumetric image as $\Gamma = \{(x, y, z) | 0 \leq x < X, 0 \leq y < Y, 0 \leq z < Z\}$. Let Φ denote a mesh of control points having dimensions $n_x \times n_y \times n_z$. The spacing δ among the control points $\phi_{i,j,k}$ is uniform. The FFD can, thus, be formulated as a 3D tensor product of 1-D cubic splines as follows:

$$T_{local}(x, y, z) = \sum_{l=0}^3 \sum_{m=0}^3 \sum_{n=0}^3 B_l(r)B_m(s)B_n(t)\phi_{i+l,j+m,k+n} \quad (1)$$

where $i = \lfloor \frac{x}{n_x} \rfloor - 1$, $j = \lfloor \frac{y}{n_y} \rfloor - 1$, $k = \lfloor \frac{z}{n_z} \rfloor - 1$, $r = \frac{x}{n_x} - \lfloor \frac{x}{n_x} \rfloor$, $s = \frac{y}{n_y} - \lfloor \frac{y}{n_y} \rfloor$, $t = \frac{z}{n_z} - \lfloor \frac{z}{n_z} \rfloor$ and where B_l represents the l^{th} basis function of the B-splines [9],

$$B_0(r) = \frac{(1-r)^3}{6} \quad (2a)$$

$$B_1(r) = \frac{3r^3 - 6r^2 + 4}{6} \quad (2b)$$

$$B_2(r) = \frac{-3r^3 + 3r^2 + 3r + 1}{6} \quad (2c)$$

$$B_3(r) = \frac{r^3}{6} \quad (2d)$$

The B-spline FFD function is parameterized by the control points Φ in a manner such that regions having a higher density of control points model regions with significant levels of local deformations, while regions in which the density of control points is low represents lower degrees of freedom of the underlying region. In order to ensure a smooth FFD based transformation, a penalty term has been used [8] as follows:

$$C_{reg} = \frac{1}{V} \int_0^X \int_0^Y \int_0^Z \left(\frac{\partial^2 \Gamma_{local}}{\partial x^2} \right)^2 + \left(\frac{\partial^2 \Gamma_{local}}{\partial y^2} \right)^2 + \left(\frac{\partial^2 \Gamma_{local}}{\partial z^2} \right)^2 + 2 \left(\frac{\partial^2 \Gamma_{local}}{\partial x \partial y} \right)^2 + 2 \left(\frac{\partial^2 \Gamma_{local}}{\partial x \partial z} \right)^2 + 2 \left(\frac{\partial^2 \Gamma_{local}}{\partial y \partial z} \right)^2 dx dy dz \quad (3)$$

where V represents the volume in the domain of the image. The similarity

measure used is sum of squared differences.

$$C_{sim} = \sum_{a=0}^{n_x} \sum_{b=0}^{n_y} \sum_{c=0}^{n_z} [I'(x+a, y+b, z+c) - I(x, y, z)]^2 \quad (4)$$

where I' represents the moving volume and I represents the reference volume. The use of sum of squared differences is justified by the fact that there is not any temporal variation in the volumetric image intensities as the registration proceeds. The overall cost function is specified as follows:

$$C(\Phi) = -C_{sim}(I, T(I')) + \lambda C_{reg}(T(I')) \quad (5)$$

where λ is the regularization weighting parameter and controls the amount of regularization of the transformation. The cost function is minimized by means of the memory efficient L-BFGS algorithm [28]. The value of λ in our case has been experimentally determined to be 0.01. The control points are evaluated in each iteration using :

$$\Phi = \Phi + \mu \frac{\nabla C}{\|\nabla C\|} \quad (6)$$

The value of μ in our case has been experimentally determined to be 0.1.

3.3. Fine Registration using Demons Algorithm

Demons algorithm [7] is applied on the output obtained from the B-splines based FFD algorithm. The Gaussian filter inherently present in the demons algorithm smooths the displacement field and removes any noise which might

have caused errors in the previous step. The principle behind the demons algorithm is that the voxels present in the reference volume would serve as local forces which would successfully displace the voxels in the moving volume in order to align it with the static volume. The displacement vector applied to each of the voxels in order to align them in an iterative manner can be written as [22]:

$$dr^{(n+1)} = \frac{(I'^{(n)} - I^{(0)})\nabla I^{(0)}}{(I'^{(n)} - I^{(0)})^2 + |\nabla I^{(0)}|^2} \quad (7)$$

In the above equation, $I'^{(n)}$ denotes the image intensity of the moving volume in the n^{th} iteration while $I^{(0)}$ denotes the image intensity of the reference volume initially. It is evident from the above equation that the gradient of the reference volume remains constant across all the iterations which saves computational time. Gaussian filter is originally used to smooth the displacement field. In the context of the present problem, the same filter additionally removes any existing noise in the control points which has possibly affected the adaptive local alignment.

3.4. FFD-Demons Synergism

Adaptive accurate registration for the present problem is achieved through the FFD-Demons synergism. The synergism is based on somewhat complementary nature of the two algorithms. B-Splines based FFD is basically an attractive model whereas Demons is a diffusive model. FFD algorithm using the B-spline grid ensures that geometrically similar points are attracted by

a set of points in the static image by a force f given by :

$$f(m, m') = \sum_{m \in I} \frac{C_{sim}(I(m), I(m'))}{h(m, m')} I(m) I(m') \quad (8)$$

where m is a voxel in the reference image, m' is a voxel in the moving image, $I(m)$ represents the intensity at point m , $h(m, m')$ is the distance between the voxels in the B-spline grid and C_{sim} is from equation (5). So, after FFD algorithm is applied, the moving image possesses a significant degree of overlap with the reference image. As the demons are being computed from the static image using the criterion $\nabla s \neq 0$, the space of transformation s is now more refined, based on FFD. The demons forces can efficiently diffuse the moving image and register it with the reference atlas while also ensuring that the model does not get trapped in a local minima from the attractive model. Thus, the synergism ensures that the diffusion of the moving image is controlled by the attractive force of FFD so that the output does not get stuck in any local minima and the noisy voxels are not diffused by the demons. The steps of the proposed method are now shown in Algorithm 1. When demons are considered for image registration, the moving image must be matched with the reference atlas by a diffusive force generated by the demon acting on an object located on the surface of the reference atlas in a manner such that the corresponding points on the moving image diffuse through the object and are accordingly aligned with the reference atlas.

Algorithm 1 Adaptive Registration Algorithm for Zebrafish Larval Images

Input: Moving Volume, Anatomical Reference Volume

Output: Registered Volume

- 1: Obtain the optimal affine transformation
Apply B-Spline based FFD on affine registered volume
 - 2: **initialize** the control points Φ
 - 3: **calculate** the gradient vector of the cost function in eq. (5) with respect to Φ
 - 4: **while** $\|\nabla C\| > \epsilon$ **do**
 - 5: **recalculate** the control points according to eq. (7).
 - 6: **recalculate** ∇C
 - 7: **increase** the density of control points adaptively
 - 8: **end while**
Apply Demons Algorithm on FFD registered volume
 - 9: **for** $i = 1$ to n **do**
 - 10: compute the displacement vector field according to eq. (8)
 - 11: **end for**
 - 12: Align the volume according to the displacement field
 - 13: **return** Registered Volume
-

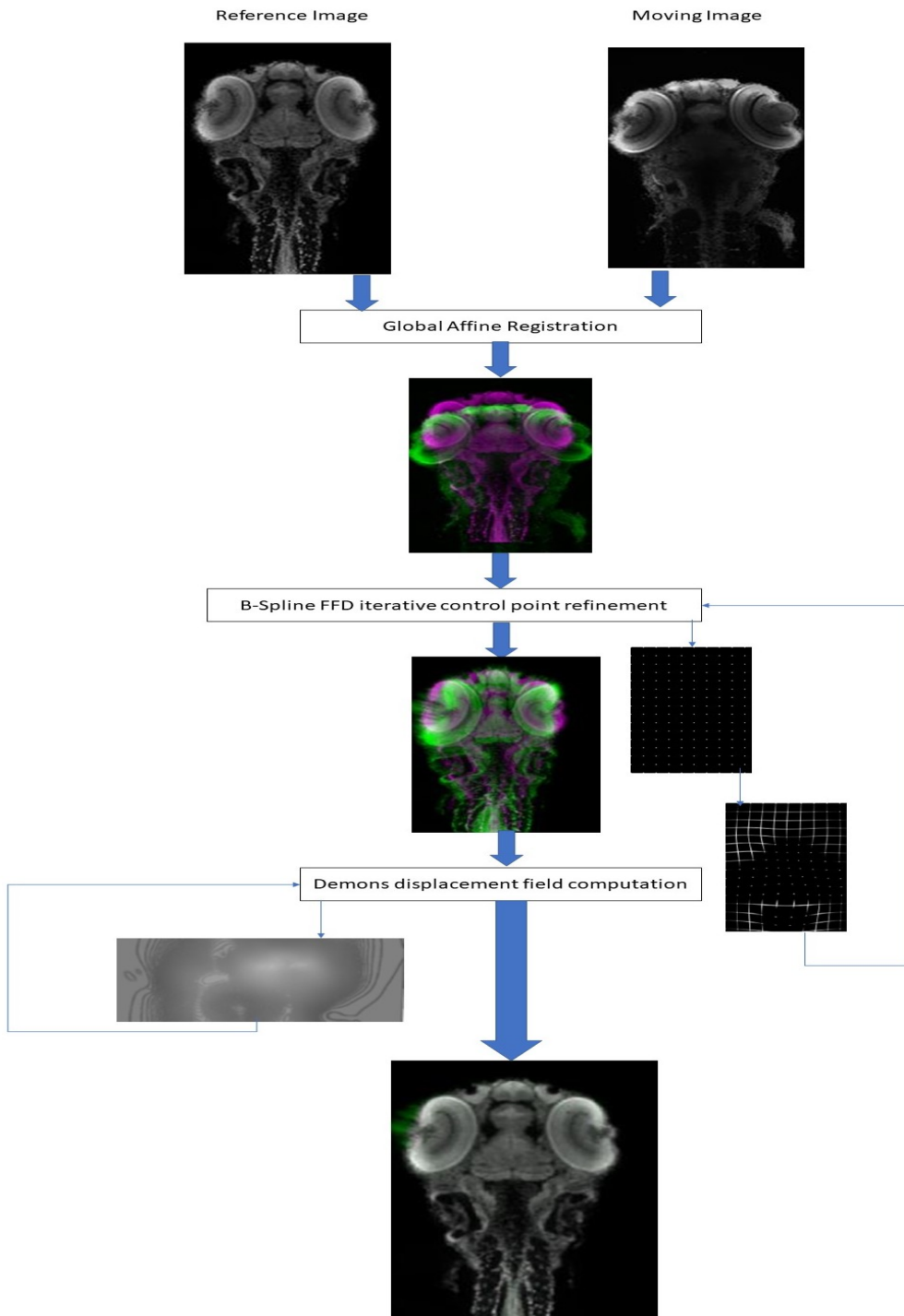


Figure 1: Flow Diagram (Zebrafish larval heads are displayed in dorsoventral view, anterior to the top)

3.5. Complexity Analysis

Let m be the number of voxels to be registered. The proposed algorithm consists of three steps, namely, the affine registration, FFD and Demons. Time-complexity of the affine registration phase of the algorithm employing the One-Plus Evolutionary optimizer is $O(m \log(m))$ [27]. FFD based adaptive spline registration with the L-BFGS optimizer runs in $O(m^2)$ time [28]. Demons algorithm is capable of solving the registration problem in linear time, *i.e.* $O(m)$ [29]. So, the overall complexity of the proposed solution is $O(m \log(m)) + O(m^2) + O(m) = O(m^2)$.

4. Experimental Results

Our experiments were performed on a dataset comprising eight multi-view confocal volumetric images of 72 hpf (hours post fertilization) zebrafish larvae to be registered on an anatomical reference (a single volumetric image). The samples were generated using the standard set of protocols for ViBE-Z sample preparation. The dimensions of the anatomical reference were $800 \times 500 \times 500$ voxels. However, the volume was scaled down to the dimensions of $200 \times 125 \times 500$ voxels as the registration was performed on a PC with Intel(R) Core(TM) i5 8th generation processor with a clock speed of 2.5 GHz.

4.1. Dataset Generation

High Quality datasets have been generated using the ViBE-Z software by the fusion of multiple confocal stacks which is required for aligning the

3D expression patterns of the different larval zebrafish at various stages of development to a common reference. The larvae used for the dataset were 72 hours post fertilization (hpf) which is an already advanced stage of development. The dataset was available in HDF5 format and could be opened using ImageJ or MATLAB R2018A. Fluorescence confocal imaging of thick samples are affected by the attenuation of the light used for excitation as well the light which is emitted. The common approximation used for modelling attenuation is that the sample is considered as a solid block with a constant attenuation coefficient. Such an approximation is too coarse for zebrafish larval head which is not a cuboid and comprises distinct local tissues and spaces filled with liquid which lead to different attenuation properties. Thus, in order to overcome these issues, ViBEZ combines the two intensity measurements available at each voxel following which it jointly estimates the local attenuation coefficient and the combined attenuation at each position in the dataset [2].

4.2. Performance Measures

The registration accuracy is measured by using Structural Similarity Index (SSIM) and Peak Signal to Noise Ratio (PSNR). The purpose of using SSIM is that it takes into account the local differences while PSNR takes into account the global differences between the registered volume and the anatomical reference. The SSIM is given by [24]:

$$SSIM(x, y) = \frac{(2\mu_x\mu_y + c_1)(2\sigma_{xy} + c_2)}{(\mu_x^2 + \mu_y^2 + c_1)(\sigma_x^2 + \sigma_y^2 + c_2)} \quad (9)$$

where, μ_x denotes the average of x , μ_y denotes the average of y , σ_x^2 denotes the variance of x , σ_y^2 denotes the variance of y , σ_{xy} denotes the covariance of x and y , $c_1 = (k_1L)^2$, $c_2 = (k_2L)^2$ are two variables to stabilize the division with weak denominator, L is the dynamic range of the pixel-values. The PSNR is given by:

$$PSNR = 10 \cdot \log_{10} \left(\frac{MAX_I^2}{MSE} \right) \quad (10)$$

where, MAX_I is the maximum possible pixel value of the image and MSE is the mean squared error. MSE is defined as follows:

$$MSE = \frac{1}{m \cdot n} \sum_{i=0}^{m-1} \sum_{j=0}^{n-1} [I(i, j) - K(i, j)]^2 \quad (11)$$

Let X and Y be two non-empty subsets of a metric space (M, d) . We define their Hausdorff distance $d_H(X, Y)$ by

$$H(X, Y) = \max\{h(X, Y), h(Y, X)\} \quad (12)$$

where

$$h(X, Y) = \max_{x \in X} \{ \min_{y \in Y} \{ d(x, y) \} \} \quad (13)$$

Given two sets, X and Y, the Dice Coefficient is defined as:

$$DSC(X, Y) = \frac{2|X \cap Y|}{|X| + |Y|} \quad (14)$$

4.3. Ablation Studies

The ablation studies depict the importance of each component of the solution pipeline. The studies also throw light into the sequence in which the algorithms need to be interleaved in order to obtain the synergistic results which exhibit a high level of overlap with the reference volume.

Table 1: SSIM Comparisons as a part of Ablation: A denotes Affine registration, B denotes B-Splines based FFD and C denotes Demons. Best values shown in **bold**.

Sl No.	Algorithm	Mean (μ) \pm Std. Dev. (σ)
1	A+B+C	0.934 \pm 0.012
2	A+B	0.642 \pm 0.054
3	A+C	0.277 \pm 0.017
4	A	0.235 \pm 0.013

Table 2: PSNR Comparisons as a part of Ablation: A denotes Affine registration, B denotes B-Splines based FFD and C denotes Demons. Best values shown in **bold**.

Sl No.	Algorithm	Mean (μ) \pm Std. Dev. (σ)
1	A+B+C	37.211 \pm 2.732
2	A+B	21.777 \pm 1.282
3	A+C	8.319 \pm 1.301
4	A	7.302 \pm 1.218

In Table 1, we present the SSIM values for various components of the

proposed solution and some combinations thereof. Similarly, in Table 2, PSNR values of the these components and same combinations are shown. The tables clearly demonstrate that removal of any component of the solution pipeline leads to a drop in the accuracy of the registration. We now show in the figures that follow, the qualitative results of the ablation studies on one sample dataset.

4.4. Comparisons with State-of-the-art Approaches

We have performed comparisons with five well-known registration algorithms. These are ViBE-Z [1], EMBC-17 [2], FFD [6], Demons [7], MSDIR [23] and ANTS [38]. The proposed method is shown to outperform all the competing methods. Our method has been further tested against a relatively recent method [23] as well which aims at performing image registration of arbitrarily ordered input images by deriving a cost function which only depends on the transformation required to warp the moving image and is independent of the atlas. The experiment has been performed parametrized with a λ value of 0.01 and optimization step size of 5. Other values have already been used but the algorithm did not show any significant changes over the values obtained with λ value of 0.01 and optimization step size of 5. ANTs [38] is an ITK based framework which essentially provides a standardized implementation of popular registration algorithms. The experiment in our case has been performed using symmetric normalization as its optimization metric having performed affine and deformable registration.

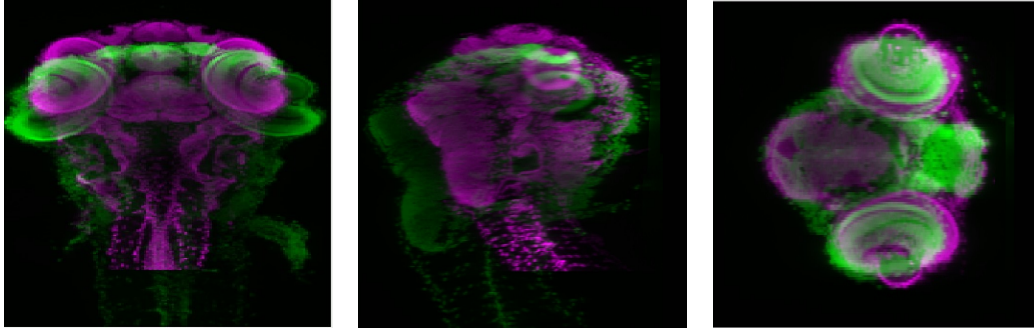


Figure 2: Unregistered images: Projection of the 3D view of the unregistered moving image (Green) overlaid on the reference image (Magenta) on different planes - See left image for XY plane, middle image for XZ plane and right image for YZ plane. Zebrafish larval heads are displayed, from left to right, in dorsoventral view (anterior to the top), lateral view (anterior to the top, ventral side to the right) and sagittal view (right side to the bottom, ventral side to the right).

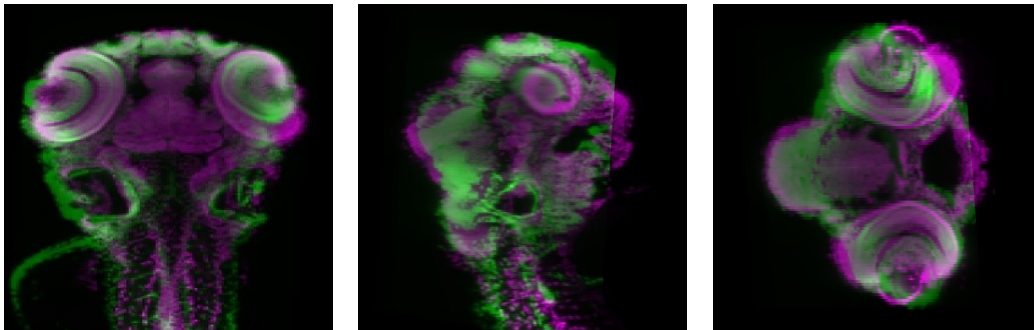


Figure 3: Affine registration: $SSIM = 0.2312$, $PSNR = 5.4324$. Projection of the 3D view of the unregistered moving image (Green) overlaid on the reference image (Magenta) on different planes - See left image for XY plane, middle image for XZ plane and right image for YZ plane. Zebrafish larval heads are displayed, from left to right, in dorsoventral view (anterior to the top), lateral view (anterior to the top, ventral side to the right) and sagittal view (right side to the bottom, ventral side to the right).

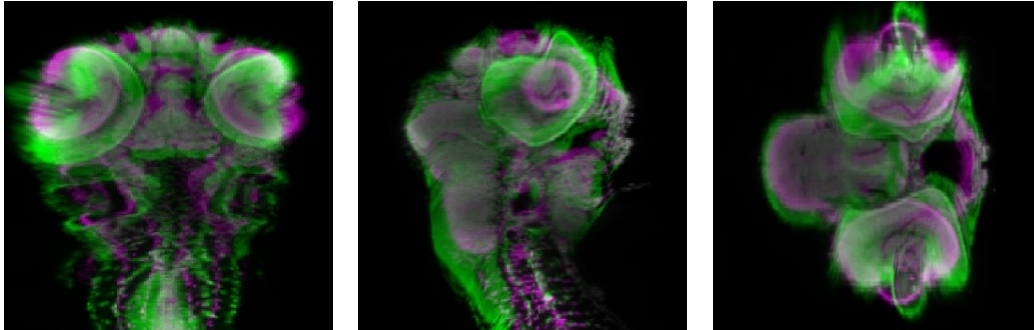


Figure 4: Affine + FFD + Demons registration: SSIM = 0.9181, PSNR = 34.7784. Projection of the 3D view of the unregistered moving image (Green) overlaid on the reference image (Magenta) on different planes - See left image for XY plane, middle image for XZ plane and right image for YZ plane. Zebrafish larval heads are displayed, from left to right, in dorsoventral view (anterior to the top), lateral view (anterior to the top, ventral side to the right) and sagittal view (right side to the bottom, ventral side to the right).

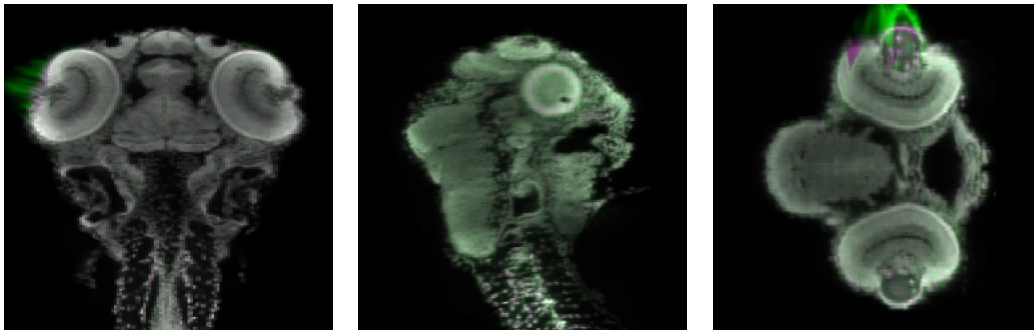


Figure 5: Affine + FFD + Demons registration: SSIM = 0.9181, PSNR = 34.7784. Projection of the 3D view of the unregistered moving image (Green) overlaid on the reference image (Magenta) on different planes - See left image for XY plane, middle image for XZ plane and right image for YZ plane. Zebrafish larval heads are displayed, from left to right, in dorsoventral view (anterior to the top), lateral view (anterior to the top, ventral side to the right) and sagittal view (right side to the bottom, ventral side to the right).

Table 3: A Comparison of SSIM Values for Various Competing Approaches. Best values are shown in **bold**.

Sl No.	Algorithm	Mean (μ) \pm S.D. (σ)	Max.	Min.
1	Ours	0.934 \pm 0.012	0.9421	0.9181
2	ViBE-Z [1]	0.717 \pm 0.057	0.7531	0.6315
3	EMBC [2]	0.748 \pm 0.010	0.7554	0.733
4	FFD [6]	0.287 \pm 0.008	0.2931	0.275
5	Demons [7]	0.248 \pm 0.010	0.2564	0.2345
6	MSDIR [23]	0.073 \pm 0.110	0.0883	0.0646
7	ANTS [38]	0.295 \pm 0.035	0.305	0.260

Table 4: A Comparison of PSNR Values for Various Competing Approaches. Best values are shown in **bold**.

Sl No.	Algorithm	Mean (μ) \pm S.D. (σ)	Max.	Min.
1	Ours	37.211 \pm 2.732	38.7223	34.7784
2	ViBE-Z [1]	20.699 \pm 1.609	22.446	19.0206
3	EMBC [2]	20.910 \pm 1.664	22.776	19.0902
4	FFD [6]	8.505 \pm 1.759	9.8175	6.0712
5	Demons [7]	7.236 \pm 1.597	8.6899	5.0716
6	MSDIR [23]	4.492 \pm 0.899	5.0919	3.1537
7	ANTS [38]	8.395 \pm 0.455	9.102	8.035

Table 5: A Comparison of Hausdorff Distance Values for Various Competing Approaches. Best values are shown in **bold**.

Sl No.	Algorithm	Mean (μ) \pm S.D. (σ)	Max.	Min.
1	Ours	401.764 \pm 2.719	403.763	401.034
2	ViBE-Z [1]	920.928 \pm 1.132	921.050	920.005
3	EMBC [2]	900.699 \pm 2.609	901.452	899.041
4	FFD [6]	1367.505 \pm 1.369	1368.4373	1366.7102
5	Demons [7]	1464.505 \pm 1.632	1465.2472	1463.5322
6	MSDIR [23]	110583.112 \pm 1.299	111582.819	110490.137
7	ANTS [38]	1163.231 \pm 2.244	1165.261	1161.748

Table 6: A Comparison of Dice Coefficient Values for Various Competing Approaches. Best values are shown in **bold**.

Sl No.	Algorithm	Mean (μ) \pm S.D. (σ)	Max.	Min.
1	Ours	0.027 \pm 0.0002	0.029	0.026
2	ViBE-Z [1]	0.025 \pm 0.001	0.026	0.024
3	EMBC [2]	0.026 \pm 0.002	0.027	0.025
4	FFD [6]	0.023 \pm 0.002	0.024	0.021
5	Demons [7]	0.021 \pm 0.003	0.023	0.019
6	MSDIR [23]	0.009 \pm 0.0005	0.010	0.008
7	ANTS [38]	0.024 \pm 0.001	0.025	0.023

In table 3, we show the SSIM values of these competing approaches. Similarly, in tables 4,5,6 we present the PSNR values, Hausdorff Distance and Dice Coefficient values respectively of these competing approaches. All the four tables clearly demonstrate that the proposed approach performs better than its competitors.

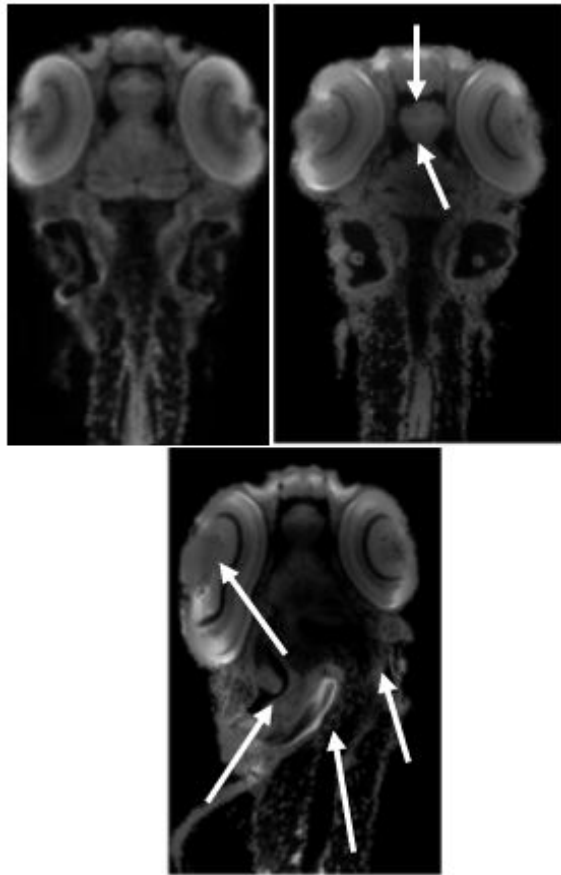


Figure 6: Qualitative comparisons of three registration algorithms: our method with SSIM = 0.9181, PSNR = 34.7784 (Top Left); [2] with SSIM = 0.7330, PSNR = 19.0902 (Top Right); [1] with SSIM = 0.6315, PSNR = 19.0206 (Bottom). Distortions resulting from [2] and [1] are depicted with white arrows. Zebrafish larval heads are displayed: on the left in dorsoventral view (anterior to the top); on top right in sagittal view (right side to the bottom, ventral side to the right); on bottom right in lateral view (anterior to the top, ventral side to the right).

In figure 6, the registration outputs of three competing algorithms are illustrated. The figure clearly portrays the superiority of the proposed solution over that of [1] and [2]. The qualitative as well as the quantitative studies show that the adaptive nature of our solution outperforms both the landmark-based approaches (e.g.[1]) as well as patch-based approaches (e.g.[2]). The reason for this significant level of improvement over the other two approaches can be attributed to the fact that our pipeline takes into consideration the varying degrees of freedom inherently present in the various regions which is modelled by the varying density of the control points. Moreover, the final step in our pipeline removes any sort of noise which might have been introduced in the control points and thus, gives a near completely accurate registration. As our solution is not dependent on detection of landmarks, which is quite difficult in low-contrast images, our results have surpassed that of [1]. In [2], Ghosal *et al.* have performed inter patch regularization by means of a weighted average which may not necessarily correct the underlying noise in the stitching across the patches. This is avoided in our algorithm as the regularization term penalizes only the non-affine transformation and moreover adaptively caters to the various regions. We have also outperformed both FFD [6] and Demons [7] when applied in isolation. This further justifies the necessity of FFD-Demons synergism. Our method also yields better results than a very recent method [23] aimed at performing image registration of arbitrarily ordered input images by deriving a cost function which only depends on the transformation required to warp the moving

image and is independent of the atlas.

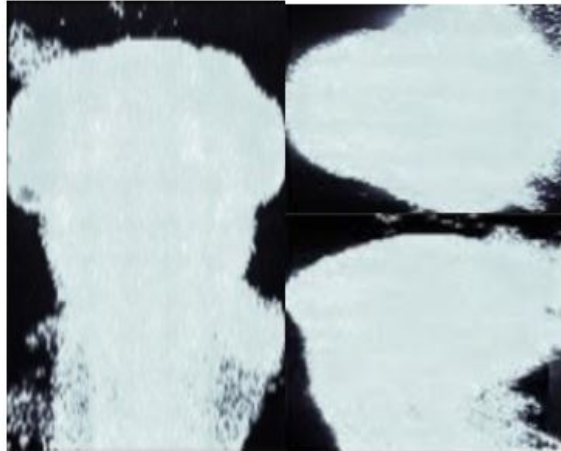


Figure 7: Projection of the 3D view of VoxelMorph [21] output. See left image for XY plane, right-top image for XZ plane and right-bottom image for YZ plane. Outputs show heavy distortions. Zebrafish larval heads are displayed: on the left in dorsoventral view (anterior to the top); on top right in sagittal view (right side to the bottom, ventral side to the right); on bottom right in lateral view (anterior to the top, ventral side to the right).

We end this section with a discussion on possible use of deep learning based VoxelMorph [21], [37] for this problem. As our dataset was extremely limited and the ground truth warp fields were also not available, we employed a transfer learning based approach in order to test our solution pipeline against the state of the art unsupervised registration algorithm, VoxelMorph. In order to apply this algorithm, the network was trained on a dataset of brain MRI scans following which the dimensions and the distributions of our dataset was made to match with those of the brain CT scans in order to use the pretrained model weights.

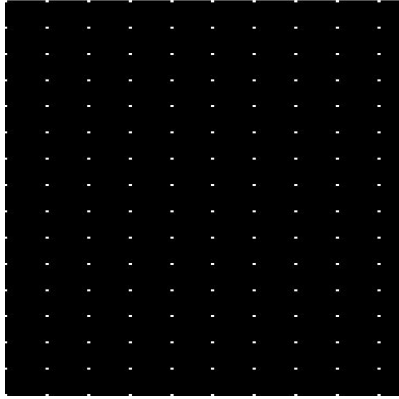
Voxelmorph determines a registration field based on the moving volumes of the brain CT scans and the weights are learned accordingly, rendering the

solution to be completely unsupervised. The registration field computed over the multiple epochs is applied on our moving volume to perform the global as well as local alignment. However, the SSIM score of the registered volume was 0.16 which is extremely poor and is evident from the registered output shown in figure 7. This can be attributed to the fact that the anatomy of a human brain is significantly different from that of a zebrafish larva owing to which the registration field estimated for the human brain would not serve as a good approximation for zebrafish larval images. Thus, we have validated that even if we use transfer learning by means of a state of the art unsupervised learning approach which outperforms most pipelines in all cases, such a solution would not be viable in our case simply because of the extreme scarcity of the number of training examples. Thus, the main challenge lies in the dataset generation in case of zebrafish larval images which is not widely available.

4.5. Robustness to Initialization

In this section, with the help of figure 8, we elucidate that the final registered volume is not sensitive to the choice of the initial control points. The nature of the solution is inherently adaptive owing to which the solution is insensitive to the nature of initialization of the control points. Following the global alignment, the localized registration is performed in which a mesh of control points is used to model the underlying deformations which act as parameters to the B-spline Free Form Deformation (FFD) function. The

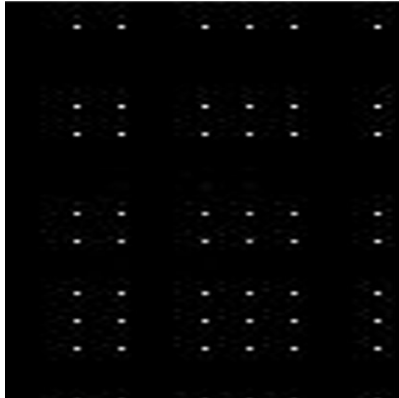
density of the control mesh increases in a coarse-to-fine fashion adaptively in accordance with the underlying geometry. As the control points model the deformations in the different regions of the zebrafish, they become inherently adaptive. So, the algorithm in itself is handling the control points in accordance with the underlying geometry without any manual intervention. Two sets of control points are chosen and the corresponding final registered volumes are shown. The values of SSIM and PSNR for the two registered volumes are very much comparable.



(a) An initial grid of control points.



(b) Final registered output SSIM = 0.9081, PSNR = 34.2014..



(c) An initial grid of control points.



(d) Final registered output SSIM = 0.9181, PSNR = 34.7784.

Figure 8: Different configurations of Control grid vs Final outputs (zebrafish larval head is displayed in dorsoventral view, anterior to the top).

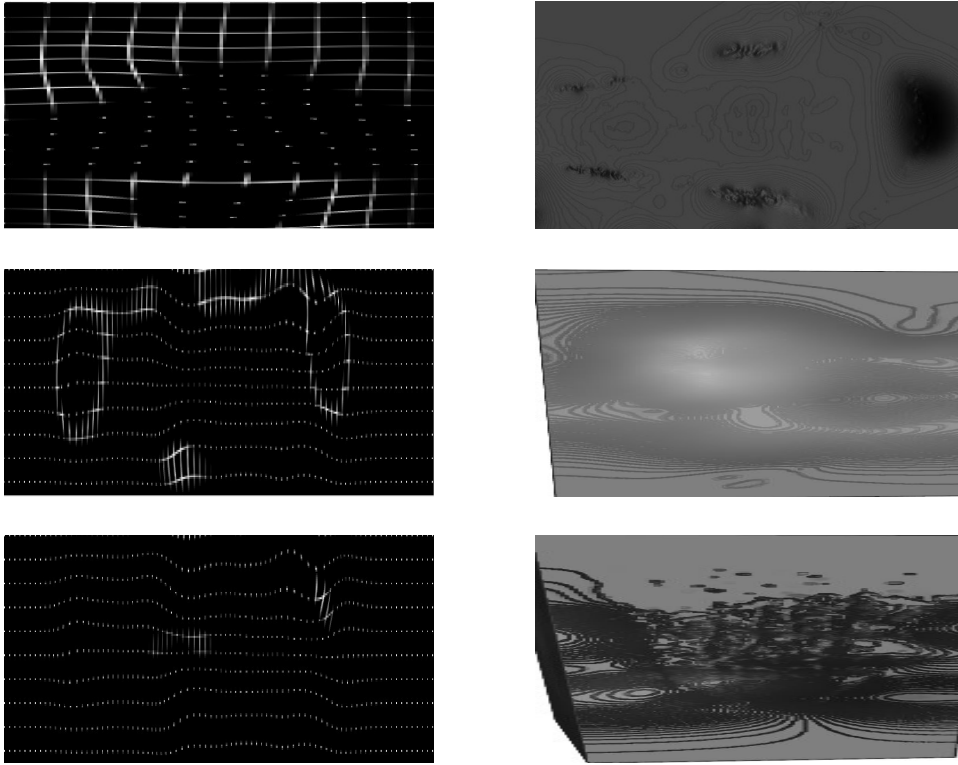


Figure 9: The warped grid in XY(top row), YZ(middle row), XZ(middle row) planes after FFD(left) & FFD-Demons(right) synergism.

4.6. Execution Time

The overall algorithm takes 20 minutes to complete on a workstation equipped with Intel(R)Core(TM)i5 8th gen processor with a clock speed of 2.5GHz having 8GB of RAM and 1TB of hard disk space. The L-BFGS optimization of the adaptive alignment takes 15 minutes to complete which comprises of a total of 15 iterations divided into 3 sets of 5 iterations each. The demons algorithm takes 100 iterations to compute the displacement field which is performed in 4 minutes. The affine registration takes the least

amount of time and is completed in approximately a minute in each of the cases. All experiments were performed in MATLAB R2018A. In table 7, we compare the execution times of several competing methods. The values show that our solution, in addition to yielding most accurate adaptive registration, is superior than [1], [2] and [23] in terms of execution times. Note that FFD in [6] used NMI and that is why it is quite time-consuming. In this work, we have applied FFD with SSD which has made it much faster.

Table 7: Execution Times of Various Competing Methods

Sl No.	Algorithm	Execution Time (min.)
1	Ours	20
2	EMBC [1]	30
3	ViBE-Z [2]	60
4	FFD [6]	15
5	Demons [7]	05
6	MSDIR [23]	120
6	ANTs [38]	05

5. Conclusion

One of the biggest challenges in the field of developmental neurology is the integration of cellular and molecular (gene expression) information, reaching a resolution sufficient to define single cells, or at least few cell diameters. So far, this level of accuracy has been quite easily obtained in invertebrate animals, but it is often hardly achievable in a vertebrate system. With the advent of ViBE-Z [1], a software developed to automatically map gene ex-

pression data to a 3D reference brain, this analysis could be extended to a vertebrate system, the zebrafish (*Danio rerio*) larva. The applicability of this software, however, requires multi-level accuracy, from signal quality to precise sample mounting and imaging. Small deformations or rotations occurring during sample preparation and acquisition, and even small variations in the pose of the larva (e.g. open or closed mouth), may make raw data inadequate for software elaboration. Sample processing and microscope set up for each acquisition are time consuming steps, with intrinsic variables due to different operators and laboratory standards. Moreover, each registration failure not only prevents the analysis of a specific gene of interest, but it also slows down the growth of a ViBE-Z-related database of key markers, shareable among an international community of neurobiologists.

In this paper, we proposed an adaptive accurate registration for Zebrafish larval images based on a synergistic combination of the FFD and the demons algorithms. Our solution explicitly uses geometry and captures varying degrees of freedom in the underlying image volumes. FFD-Demons synergism builds an effective combination of an attractive and a diffusive registration model. The experimental results validate the superiority of our solution over other approaches and also establish the necessity of each component in the pipeline. In future, if a larger labeled dataset of zebrafish larval images is made available or alternatively be synthesized, a deep learning based approach for further improving the solution can be explored.

Acknowledgement

The authors wish to thank Prof. W. Driever, at the University of Freiburg, Germany for his continuous support on the development of the Vibe-Z system. Natascia Tiso was supported by the Telethon grant GGP19287 and the AIRC grant IG-2017-19928.

References

- [1] O. Ronneberger et al., “Vibe-z: a framework for 3d virtual colocalization analysis in zebrafish larval brains,” *Nat. Methods*, Vol. 9, pp. 735–742, 2012.
- [2] S. Ghosal, S. Banerjee, N. Tiso, E. Grisan and A. S. Chowdhury, “A novel non-rigid registration algorithm for zebrafish larval images,” In *Proc. EMBC*, pp. 321-324, 2017.
- [3] T. Annala et al., “Zebiat, an image analysis tool for registering zebrafish embryos and quantifying cancer metastasis,” *BMC Bioinf.*, Vol. 14(Suppl 10):S5, pp. 1–9, 2013.
- [4] A. Bhalerao et al., “Local affine texture tracking for serial registration of zebrafish images,” *Proc. ISBI*, pp. 434–437, 2012.
- [5] Styner, M., C. Brechbuehler, G. Székely, and G. Gerig. “Parametric estimate of intensity inhomogeneities applied to MRI,” *IEEE Trans. Med. Imaging*, Vol. 19, No. 3, 2000, pp. 153-165.

- [6] D. Rueckert, L. I. Sonoda, C. Hayes, D. L. G. Hill, M. O. Leach and D. J. Hawkes, “Nonrigid registration using free-form deformations: application to breast MR images,” *IEEE Trans. Med. Imaging*, Vol. 18, No. 8, pp. 712-721, Aug. 1999.
- [7] Thirion, J.-P. “Image matching as a diffusion process: an analogy with Maxwell’s demons”. *Med. Image Anal.*, Vol. 2, No. 3, 1998, pp. 243–260.
- [8] G. Wahba, “Spline models for observational data,” *Soc. Industr. Applied Math.*, 1990.
- [9] S. Lee, G. Wolberg, K.-Y. Chwa, and S. Y. Shin, “Image metamorphosis with scattered feature constraints,” *IEEE Trans. Vis. Comput. Graph.*, Vol. 2, pp. 337–354, Oct. 1996.
- [10] R.E. Blaser, D.G. Vira, “Experiments on learning in zebrafish (*Danio rerio*): A promising model of neurocognitive function,” *Neuroscience & Biobehavioral Rev.*, Vol. 42, pp. 224-231, 2014.
- [11] B. B. Avants, C. L. Epstein, M. Grossman, and J. C. Gee, “Symmetric diffeomorphic image registration with cross-correlation: evaluating automated labeling of elderly and neurodegenerative brain,” *Med. Image Anal.*, Vol. 12, No. 1, pp. 26–41, 2008
- [12] J. Ashburner, “A fast diffeomorphic image registration algorithm,” *Neuroimage*, Vol. 38, No. 1, pp. 95–113, 2007.

- [13] A. V. Dalca, A. Bobu, N. S. Rost, and P. Golland, “Patch-based discrete registration of clinical brain images,” in Proc. Patch-MI, pp. 60–67, 2016.
- [14] B. T. Yeo, M. R. Sabuncu, T. Vercauteren, D. J. Holt, K. Amunts, K. Zilles, P. Golland, and B. Fischl, “Learning task-optimal registration cost functions for localizing cytoarchitecture and function in the cerebral cortex,” *IEEE Trans. Med. imaging*, Vol. 29, No. 7, pp. 1424–1441, 2010.
- [15] M. Zhang, R. Liao, A. V. Dalca, E. A. Turk, J. Luo, P. E. Grant, and P. Golland, “Frequency diffeomorphisms for efficient image registration,” in Proc. IPMI, pp. 559–570, 2017.
- [16] X. Cao, J. Yang, J. Zhang, D. Nie, M. Kim, Q. Wang, and D. Shen, “Deformable image registration based on similarity-steered cnn regression,” in Proc. MICCAI, pp. 300–308, 2017.
- [17] J. Krebs, T. Mansi, H. Delingette, L. Zhang, F. C. Ghesu, S. Miao, A. K. Maier, N. Ayache, R. Liao, and A. Kamen, “Robust non-rigid registration through agent-based action learning,” in Proc. MICCAI, pp. 344–352, 2017.
- [18] M.-M. Rohe, M. Datar, T. Heimann, M. Sermesant, and X. Pennec, “Svf-net: Learning deformable image registration using shape matching,” in Proc. MICCAI, pp. 266–274, 2017.
- [19] H. Sokooti, B. de Vos, F. Berendsen, B. P. Lelieveldt, I. Isgum, and M.

- Staring, “Nonrigid image registration using multi-scale 3d convolutional neural networks,” in Proc. MICCAI, pp. 232–239, 2017.
- [20] X. Yang, R. Kwitt, M. Styner, and M. Niethammer, “Quicksilver: Fast predictive image registration—a deep learning approach,” *NeuroImage*, vol. 158, pp. 378–396, 2017.
- [21] Guha Balakrishnan, Amy Zhao, Mert R. Sabuncu, John Guttag, and Adrian V. Dalca “VoxelMorph: A Learning Framework for Deformable Medical Image Registration,” *IEEE Trans. Med. Imaging*, Vol. 38, No. 8, pp. 1788–1800, 2019.
- [22] Gu X, Pan H, Liang Y, et al. Implementation and evaluation of various demons deformable image registration algorithms on a GPU. *Phys Med Biol*. 2010;55(1):207-219.
- [23] I. Aganj, J.E. Iglesias, M. Reuter, M. R. Sabuncu, and B. Fischl, “Mid-space-independent deformable image registration,” *NeuroImage*, Vol. 152, pp. 158-170, 2017.
- [24] Brunet, Dominique. “A Study of the Structural Similarity Image Quality Measure with Applications to Image Processing,” *Doctoral dissertation*, University of Waterloo, Ontario, Canada, 2012.
- [25] Roberto M. Dyke, Yu-Kun Lai, Paul L. Rosin, and Gary K.L. Tam, “Non-rigid registration under anisotropic deformations,” *Computer Aided Geom. Des.*, Vol. 71, pp. 142-156, 2019.

- [26] Takehiro Kajihara, Takuya Funatomi, Haruyuki Makishima, Takahito Aoto, Hiroyuki Kubo, Shigehito Yamada, and Yasuhiro Mukaigawa, “Non-rigid registration of serial section images by blending transforms for 3D reconstruction,” *Pattern Recognit.*, Vol. 96, 106956, 2019.
- [27] Jun He, Xin Yao, Drift analysis and average time complexity of evolutionary algorithms, *Artif. Intel.*, Vol. 127, No. 1, pp. 57-85, 2001.
- [28] Schraudolph, Nicol N and Yu, Jin and Günter, Simon, A stochastic quasi-Newton method for online convex optimization, *Proc. AISTATS*, pp. 436-443, 2007.
- [29] Cahill N.D., Noble J.A., Hawkes D.J. (2009) A Demons Algorithm for Image Registration with Locally Adaptive Regularization, In *Proc. MICCAI*, pp. 574 - 581, 2009.
- [30] Tang, Z. and Yap, P.T. and Shen, D., “A New Image Similarity Metric for Improving Deformation Consistency in Graph-Based Groupwise Image Registration”, *IEEE Trans. Biomed. Eng.*, Vol. 66, No. 8, pp. 2192-2199, 2018.
- [31] Lotz, Johannes *et al.*, “Patch-based nonlinear image registration for gigapixel whole slide images”, *IEEE Trans. Biomed. Eng.*, Vol. 63, No. 9, pp. 1812-1819, 2015.
- [32] Rahmani Moghadam and Y. -P. P. Chen, ”Tracking Neutrophil Migration in Zebrafish Model Using Multi-Channel Feature Learn-

- ing,” in IEEE Journal of Biomedical and Health Informatics, doi: 10.1109/JBHI.2020.3019271.
- [33] Kunst M, Laurell E, Mokayes N, Kramer A, Kubo F, Fernandes AM, Förster D, Dal Maschio M, Baier H. A Cellular-Resolution Atlas of the Larval Zebrafish Brain. *Neuron*. 2019 Jul 3;103(1):21-38.e5. doi: 10.1016/j.neuron.2019.04.034. Epub 2019 May 27. PMID: 31147152.
- [34] Tambalo M, Mitter R, Wilkinson DG. A single cell transcriptome atlas of the developing zebrafish hindbrain. *Development*. 2020 Mar 16;147(6):dev184143. doi: 10.1242/dev.184143. PMID: 32094115; PMCID: PMC7097387.
- [35] Arnim Jenett, Chapter 32 - Registered, standardized, and interactive: a review of online resources for zebrafish neuroanatomy, Editor(s): Robert T. Gerlai, *Behavioral and Neural Genetics of Zebrafish*, Academic Press, 2020, Pages 563-580, ISBN 9780128175286
- [36] G. M. Fleishman et al., ”Deformable Registration of Whole Brain Zebrafish Microscopy Using an Implementation of the Flash Algorithm Within Ants,” 2019 IEEE 16th International Symposium on Biomedical Imaging (ISBI 2019), Venice, Italy, 2019, pp. 213-217, doi: 10.1109/ISBI.2019.8759549.
- [37] Tingxi Wen, Haotian Liu, Luxin Lin, Bin Wang, Jigong Hou, Chuanbo Huang, Ting Pan, Yu Du, Multiswarm Artificial Bee Colony algorithm

based on spark cloud computing platform for medical image registration, Computer Methods and Programs in Biomedicine, Volume 192, 2020, 105432, ISSN 0169-2607

- [38] Avants BB, Tustison NJ, Stauffer M, Song G, Wu B, Gee JC. The Insight ToolKit image registration framework. Front Neuroinform. 2014 Apr 28;8:44. doi: 10.3389/fninf.2014.00044. PMID: 24817849; PMCID: PMC4009425.
- [39] Chetverikov, Dmitry et al. "The Trimmed Iterative Closest Point algorithm." Object recognition supported by user interaction for service robots 3 (2002): 545-548 vol.3.
- [40] T. Wan et al., "RGB-D Point Cloud Registration Based on Salient Object Detection," in IEEE Transactions on Neural Networks and Learning Systems, doi: 10.1109/TNNLS.2021.3053274.
- [41] haoyi Du, Guanglin Xu, Sirui Zhang, Xuetao Zhang, Yue Gao, Badong Chen, Robust rigid registration algorithm based on pointwise correspondence and correntropy, Pattern Recognition Letters, Volume 132, 2020, Pages 91-98, ISSN 0167-8655,
- [42] Sarlin, Paul-Edouard & DeTone, Daniel & Malisiewicz, Tomasz & Rabinovich, Andrew. (2020). SuperGlue: Learning Feature Matching With Graph Neural Networks. 4937-4946.